

Numerical Simulation of Turbidity Current Using $\overline{v^2} - f$ Turbulence Model

A. Mehdizadeh¹, B. Firoozabadi² and B. Farhanieh³

¹ Graduate Student, Mechanical Eng. Dept, Sharif University of Technology, Azadi Ave., Tehran, Iran

² Associate Professor, Mechanical Eng. Dept, Sharif University of Technology, Azadi Ave., Tehran, Iran,

³ Professor, Mechanical Eng. Dept, Sharif University of Technology, Azadi Ave., Tehran, Iran,

Email: firoozabadi@sharif.edu

(Received April 9, 2007; accepted November 28, 2007)

ABSTRACT

The deposition behavior of fine sediment is an important phenomenon, and yet unclear to engineers concerned about reservoir sedimentation. An elliptic relaxation turbulence model ($\overline{v^2} - f$ model) has been used to simulate the motion of turbid density currents laden with fine solid particles. During the last few years, the $\overline{v^2} - f$ turbulence model has become increasingly popular due to its ability to account for near-wall damping without use of damping functions. The $\overline{v^2} - f$ model has also proved to be superior to other RANS (Reynolds-Averaged Navier-Stokes) methods in many fluid flows where complex flow features are present. This current becomes turbulent at low Reynolds number (order 1000). The $k - \varepsilon$ model, which was standardized for high Reynolds number and isotropic turbulence flow, cannot simulate the anisotropy and non-homogenous behavior near the wall. In this study, the turbidity current with a uniform velocity and concentration enters the channel via a sluice gate into a lighter ambient fluid and moves forward down-slope. The model has been validated by available experimental data sets. Moreover, results have been compared with the standard $k - \varepsilon$ turbulence model. The deposition of particles and the effects of their fall velocity on concentration distribution, Richardson number, and the deposition rate are also investigated. The results show that the coarse particles settle rapidly and make the deposition rate higher.

Keywords: Density Current, Turbulence modeling, V2-f turbulence model.

NOMENCLATURE

b_0	width of the layer	T	time scale of turbulence
C	concentration	U_{ave}	layer-averaged velocity in the x direction
$C_\mu, C_{\varepsilon 1}, C_{\varepsilon 2}$	empirical constants in the $k - \varepsilon$ model	u, v	time-averaged velocity components in the x and y directions, respectively;
E	water entrainment coefficient	u^*	shear velocity
f	relaxation variable	$u_i u_j$	Reynolds stresses
f_μ	damping function	v_f	sediment particle fall velocity
g	gravity	y	wall normal distance
g'	reduced gravity	ρ_w	density of water;
h	density currents height	ε	energy dissipation rate
H	water depth	ρ_s	density of particles
k	turbulent kinetic energy	θ	channel slope angle in degree.
L	length scale of turbulence	$\overline{v^2}$	turbulent velocity scale
P	pressure	κ	von Karman constant;
P_k	production term	ν_t	turbulence viscosity;
Ri	bulk Richardson number	σ_k and σ_ε	turbulence constants
S	$S^2 = S_{ij} S_{ij}$		
S_{ij}	strain rate tensor		

1. INTRODUCTION

Turbid water from river, into the reservoir often goes below the strata of clear water and produces a phenomenon known as “turbid density current”. These currents are quite different from the free jet flows and river sediment transportation. Such flows are only produced due to the vertical density gradient. In fact, the magnitude of the driving force and the corresponding velocity is directly proportional to the density gradient (Firoozabadi *et al.*, 2003).

Turbidity currents are continuous flows, which move down the slope because of the gravity due to the fact that, their density is heavier than ambient water. Generally speaking, density differences in these currents can arise from temperature differences, different chemical species, suspended solids, and etc.. Turbidity currents in the ocean are known to be a maker of submarine canyons (Fan and Morris, 1992; Salaheldin *et al.*, 2000). Thunderstorm and the winds are density currents in the atmosphere formed by hot and cold air. Gulf Stream and oil spillage represent other forms of density currents. Some of experimental studies in the literatures on density or turbidity currents are Ellison and Turner (1959), Rad (1976), Alavian (1986), Parker *et al.* (1987), Garcia (1993), Altinakar *et al.* (1996), and Lee and Yu (1997).

Mainly, there are two modeling techniques are available for exploring density currents numerically, namely, the vertical structure model, and the integral model. The vertical structure model uses Reynolds equations as well as a turbulence closure model to find the flow variables that are non-uniform over the depth.

This approach widely can be found in the references, Stacey and Bowen (1988a, b), who used a mixing length model for the turbulence closure. Eidsvik and Brors (1989) applied the $k-\varepsilon$ turbulence model to turbidity currents. Using the Reynolds stress model the vertical structure of turbidity currents has also been studied in Brors and Eidsvik (1992). Density currents which occur in sedimentation tanks have been simulated by the $k-\varepsilon$ turbulence model in Lyn *et al.* (1992) and Lakehal *et al.* (1999). Low Reynolds number turbulent model ($k-\varepsilon$ Launder-Sharma) was employed by Firoozabadi *et al.* (2000) to investigate the structure of this current.

In all the efforts, which used $k-\varepsilon$ or modified $k-\varepsilon$ model for the low Reynolds number flows, the result showed the poor agreement with the experimental data, and if not, that work applied the experimental correlation, to model the shear velocity or entrainment coefficient. This weakness comes from the weak points of the $k-\varepsilon$ model, which cannot simulate accurately the behavior near the wall (e.g. over-prediction in eddy viscosity near the wall) and

lack of the ability to simulate the anisotropy effects in the domain.

In the last few years, the $\overline{v^2-f}$ turbulence model, originally suggested by Durbin (1991), has become increasingly popular due to its ability to correctly account for near-wall damping without the use of damping functions. The $\overline{v^2-f}$ model has shown its strong ability in many fluid flows where complex flow features are present and be superior to other RANS (Reynolds-Averaged Navier-Stokes) methods. For example, Parneix *et al.* (1998) successfully computed the strong three-dimensional flow around a wall-mounted appendage. Using the $\overline{v^2-f}$ model Hermanson *et al.* (2003) obtained improvements in the predicted heat transfer rates as compared to the $k-\varepsilon$ computations for a stator vane flow. Similar results were also found in Sveningsson (2003). Another class of flows where the $\overline{v^2-f}$ model seems to work well is separated flows. Cokljat *et al.* (2003) computed a set of recirculating flows and found that the $\overline{v^2-f}$ model in most cases outperformed two-equation approaches. The same trend was seen in Iaccarino (2001) where the flow in an asymmetric diffuser was computed using the $\overline{v^2-f}$ model and the Launder-Sharma low-Reynolds number $k-\varepsilon$ model. The separation bubble characteristic of this flow was fairly accurately predicted with the $\overline{v^2-f}$ model whereas the $k-\varepsilon$ model produced no recirculation at all. Due to the somewhat unstable formulation of the wall boundary condition of the relaxation parameter, f , in the original formulation of the $\overline{v^2-f}$ model, Lien and Kalitzin (2001) slightly redefined f in order to have a numerically more attractive boundary condition. Due to the improved numerical properties of the redefined model, it has become more popular than the original, which in most cases requires a coupled solution procedure (e.g. Sveningsson, 2003). In the recent studying of Sveningsson (2004), the behavior of two versions of the $\overline{v^2-f}$ model is compared in an attempt to investigate in what aspects they differ and also to improve the overall understanding of the $\overline{v^2-f}$ models performance.

In this study, the two-dimensional turbidity current was simulated with improved $\overline{v^2-f}$ model (Lien *et al.* 2001) to identify the ability of this model in these especial types of currents. This study, which is compared with the different experimental data sets, involves an accurate procedure that can accurately calculate the behaviors of the turbidity current.

2. MATHEMATICAL MODELING

2.1 Governing equations

Figure 1 shows the schematic sketch of turbidity current. The concentration of turbid-water is so small that Boussinesq approximation can be used with this

assumption; the effect of density difference are neglected in the inertia term, but included in the buoyancy force term. Thus, the governing equations for the steady state turbidity current are

$$\frac{\partial u}{\partial x} + \frac{\partial v}{\partial y} = 0 \quad (1)$$

$$u \frac{\partial u}{\partial x} + v \frac{\partial u}{\partial y} = -\left(\frac{1}{\rho}\right) \frac{\partial P}{\partial x} + g' \sin\theta + \frac{\partial}{\partial y}(\nu + \nu_t) \frac{\partial u}{\partial y} \quad (2)$$

$$u \frac{\partial v}{\partial x} + v \frac{\partial v}{\partial y} = -\left(\frac{1}{\rho}\right) \frac{\partial P}{\partial y} - g' \cos\theta + \frac{\partial}{\partial y}(\nu + \nu_t) \frac{\partial v}{\partial y} \quad (3)$$

$$u \frac{\partial C}{\partial x} + v \frac{\partial C}{\partial y} = \frac{\partial}{\partial y}(\lambda + \zeta_s) \frac{\partial C}{\partial y} + \nu_f \cos\theta \frac{\partial C}{\partial y} \quad (4)$$

where these equations are, continuity, momentum and mass balances. C is the concentration of the dense fluid defined as $C = (\rho - \rho_w) / (\rho_s - \rho_w)$ and ρ is the density of the mixture. ρ_s and ρ_w are the particles and water density, respectively. ν and λ are the viscosity and diffusivity of fluid, respectively. In the momentum equation, g' is the reduced gravitational acceleration

$$g' = g \frac{\rho - \rho_w}{\rho_w} \quad (5)$$

In the concentration equation, ν_f is the particles fall velocity and ζ_s is the turbulence diffusivity. By using the turbulent Schmidt number Sc , eddy diffusivity will be

$$\zeta_s = \frac{\nu_t}{Sc} \quad (6)$$

While the Schmidt number, similar to the Prandtl number, is affected by the buoyancy, there is assumed to be unity here (Lyn *et al.* 1992). The particles in the current are assumed dilute and non-cohesive with equal settling velocities. The pressure term is defined as

$$\frac{P}{\rho_w} = \frac{P_o}{\rho_w} - g'(H - h) + \rho g(H - y) / \rho_w \quad (7)$$

p_o is the surface pressure and H, h are the water depth and density current height, respectively. Due to entrainment in the turbid density current, the height and the average density of turbidity current change continuously. Therefore, the pressure gradient cannot be omitted.

It's worth mentioning that in the laboratory, a gate valve controls the feed rate, and the feed rate is fixed at a desired rate. Thus, the current would be in a quasi-steady condition and we considered a steady state condition in the present work.

2.2 Turbulence modeling

Most of CFD packages use the standard or modified versions of the $k - \varepsilon$ turbulence model. Physical phenomena involved in the turbidity current are substantially different and have been considered as highly challenging test cases for the validation of turbulence models. Since near the wall region in this current is very important, the turbidity current lies on the bed and has a

short height from the bed, thus causing a near bed behavior to have the important effect on the characteristics of the current, but the standard $k - \varepsilon$ model showed a poor result in this region (Parneix 1998, Lander 1974). Moreover, this current becomes turbulent at a low Reynolds number (order 1000); hence, the $k - \varepsilon$ model which has been standardized for a high Reynolds number and an isotropic turbulence flow, cannot simulate the anisotropy and non-homogenous behavior near the wall as well as shear layer (Durbin 1995, Parneix 1998). In order to integrate $k - \varepsilon$ into the wall, it is common practice to introduce the low-Reynolds number damping functions. These turn to mimic certain near-wall behaviors (Launder and Sharma, 1974). However, all these models use a single-point approach (Durbin and Pettersson 2001) that cannot represent the non-local effects of pressure-reflection that occur near solid boundaries. In many cases, these damping functions involve an ill-defined normal distance to the wall, which cannot be used in complex geometries. They are also highly non-linear and sometimes introduce numerical rigidity.

An attractive alternative to the $k - \varepsilon$ model is the $\overline{v^2} - f$ turbulence model (Durbin *et al.* 1991). By considering the exact transport equations for the Reynolds stresses in a fully developed channel flow, it can readily be shown that the production of \overline{uv} (the only Reynolds stress component that affects the mean flow field) should be proportional to $\overline{v^2}$. In two-equation models, this velocity scale (squared) is not explicitly available, but is replaced by the turbulence kinetic energy k . As k has a different wall distance dependency (y^2) from $\overline{v^2}$ (y^4), this modeling is expected to be inaccurate as walls are approached. This deficiency can be controlled to some extent by introducing a damping function that improves the wall distance dependency of \overline{uv} . Durbin (1991) showed that by simply replacing k with $\overline{v^2}$ in the definition of the eddy-viscosity, results were substantially improved. Hence, an alternative interpretation, or definition of the damping function, say f_μ , is $\overline{v^2} = f_\mu k$.

The main problem with a damping function is that this function can be tuned to only a limited number of test cases. In $\overline{v^2} - f$ model, on the other hand, $\overline{v^2}$ is governed by a separate transport equation and thus, has a potential of being applicable to a wider range of flow situations. In general, $\overline{v^2}$ should be regarded as a scale for the velocity component responsible for turbulent transport which is proportional to k far from solid walls.

While in the near-wall region, $\overline{v^2}$ becomes the velocity fluctuation normal to the solid surface, regardless of the orientation of the surface. One important feature of the $\overline{v^2}$ equation is its ability to account for non-local effects (e.g. kinematics blocking) by solving an elliptic relaxation equation for f , a parameter closely related to the

pressure strain redistribution term. A modified Helmholtz operator introduces ellipticity, which is amenable to numerical computations. It introduces wall effects by a linear equation. This operator generates turbulence profiles that evolve from the near-wall behavior to form suitable areas far from the solid boundaries. Finally, a mathematical constraint has been added to prevent non-reliability of the eddy viscosity especially in the stagnation region (Durbin *et al.* 1996).

For an extensive discussion on this subject, see Manceau *et al.* (2001). The model equations are outlined as follows. The $\overline{v^2} - f$ model could be thought of as a simplification of a full Second Moment Closure (SMC) model (Durbin, 1993). For instance, the source terms in f equation represent a return to isotropy and isotropization models for energy redistribution. In this and other ways, important effects of near-wall anisotropy are represented. However, the $\overline{v^2} - f$ model has the advantage of solving the mean flow with an eddy viscosity, which avoids some computational stability problems encountered with the full SMC models. It is a general geometry turbulence model, valid right up to solid walls. It does not need wall functions whose universality is increasingly being called into question (Behnia *et al.* 1999).

In the modified $\overline{v^2} - f$ turbulence model the following transport equations must be solved in order to estimate eddy viscosity

$$U_j \frac{\partial k}{\partial x_j} = \frac{\partial}{\partial x_j} \left((v + \frac{v_t}{\sigma_k}) \frac{\partial k}{\partial x_j} \right) + p_k - \varepsilon \quad (8)$$

$$U_j \frac{\partial \varepsilon}{\partial x_j} = \frac{\partial}{\partial x_j} \left((v + \frac{v_t}{\sigma_k}) \frac{\partial \varepsilon}{\partial x_j} \right) + \frac{C_{\varepsilon 1} p - C_{\varepsilon 2} \varepsilon}{T} \quad (9)$$

$$U \cdot \nabla \overline{v^2} = \frac{1}{\rho} \nabla \cdot [(\mu + \frac{\mu_t}{\sigma_k}) \nabla \overline{v^2}] + k \tilde{f} - 6 \frac{\varepsilon \overline{v^2}}{k} \quad (10)$$

where $U_j = (u, v, 0)$; k , turbulence kinetic energy; ε , dissipation; μ, μ_t are dynamic and turbulence viscosity, respectively; and v_t is defined as $v_t = \frac{\mu_t}{\rho}$.

Furthermore the below elliptic equation must be solved (f equation)

$$\tilde{f} - L^2 \nabla^2 \tilde{f} = \frac{c_1}{T} \left[\frac{2}{3} - \frac{\overline{v^2}}{k} \right] + C_2 \frac{P_k}{k} + 5 \frac{\overline{v^2}}{kT} \quad (11)$$

In these equations production term is $P_k = v_t \left(\frac{\partial U_i}{\partial x_j} + \frac{\partial U_j}{\partial x_i} \right) \frac{\partial U_i}{\partial x_j}$ and v_t , the eddy viscosity is

defined as $v_t = C_\mu \overline{v^2} T$ in which $C_\mu = 0.09$. The source term on the right side of the f -equation is analogous to the IP from closure model. The constants are $C_1=0.4, C_2=0.3$. The length scale (L) and time scale (T) in these equations are introduced as

$$L = C_L \max \left\{ L', C_\eta \left(\frac{v^3}{\varepsilon} \right)^{1/4} \right\} \quad (12)$$

$$L' = \min \left\{ \frac{k^{3/2}}{\varepsilon}, \frac{1}{\sqrt{3}} \frac{k^{3/2}}{C_\mu v^2 \sqrt{2S^2}} \right\} \quad (13)$$

$$T = \min \left\{ T', \frac{0.6}{\sqrt{3}} \frac{k}{C_\mu v^2 \sqrt{2S^2}} \right\} \quad (14)$$

$$T' = \max \left\{ \frac{k}{\varepsilon}, 6 \left(\frac{v}{\varepsilon} \right)^{1/2} \right\} \quad (15)$$

where $S = S_{ij} S_{ij}$ and $S_{ij} = \frac{1}{2} \left(\frac{\partial U_i}{\partial x_j} + \frac{\partial U_j}{\partial x_i} \right)$. The $\overline{v^2} - f$

model requires values of k and ε . They are determined by their equations, the only revision being to replace $C_{\varepsilon 1}$

either by $1.41 \left[1 + 0.045 \sqrt{k/\overline{v^2}} \right]$ or by

$$1.3 + 0.25 \left[1 + (0.15d/L)^2 \right]^{\frac{1}{4}} \quad (\text{Parneix } et al. 1998).$$

Either one of these increases the dissipation near the wall and improves the predictions of k .

2.3 Test case and boundary conditions

The computational domain was defined based on the two-dimensional laboratory experiments of Choi and Garcia (2002) and Akiyama *et al.* (1994). The boundary conditions at the inlet are known. Similar to the experimental models, the kaolin-laden flow with uniform velocity and concentration enters the channel under the still bodies of water passing through a sluice gate, on the bed inclined at angle θ . At the out-flow boundary, the stream-wise gradients of all variables are set to zero. It is expected that modeling of the outlet have only a local effect on the flow field. When the effects of wind and small ripples on the flow field can be neglected, at the free surface, the rigid-lid approximation can be imposed (Firoozabadi *et al.*, 2003, Bournet *et al.*, 1999). Then the symmetry condition is applied that includes zero gradients (zero shears) and zero fluxes perpendicular to the boundary. At the rigid walls, due to the no-slip conditions and a pure depositing assumption, the velocities and concentration gradients are set to zero. For particles mass balance equation, zero gradient conditions normal to the vertical wall are applied. Also for the $k - \varepsilon$ and modified $\overline{v^2} - f$ equations, at the free surface, no flux

conditions are imposed, i.e., $\frac{\partial k}{\partial y} = \frac{\partial \varepsilon}{\partial y} = \frac{\partial \overline{v^2}}{\partial y} = \frac{\partial f}{\partial y} = 0$

and at the inlet $k_{ent} = (0.1u_{int})^2$ and

$\varepsilon_{ent} = k_{ent}^{3/2} C_\mu^{3/4} / KL$ in which K is the Von-Karman constant.

2.4 Solution procedure

The flow and the turbulent equations have to be accurately resolved to obtain the concentration distribution predictions. All computations were performed in Cartesian coordinates with rectangular geometry. Cartesian grids were used, with a high resolution near all solid boundaries.

In all cases (for the $\overline{v^2} - f$ model), the first grid point was at $y^+ \approx 1$ or less (Behnia *et al.* 1999). Therefore, the solutions presented here are considered grid independent (Behnia *et al.* 1999). However, for both models, the grid independency study was utilized and some tests were performed with different grid sizes to seek a grid independent solution in each test case. The mesh points were chosen as uniform in the streamwise direction, but in the vertical direction, because of high gradients in the near-bed region, the grid points were distributed in a non-uniform manner with a higher density of grids close to the bed.

2.5 Solver

A finite volume code was developed by using the pressure correction scheme SIMPLEX and a collocated grid arrangement with Rhie-Chow (1983) interpolation. The hybrid scheme was used for discretizing the momentum, turbulence and particles mass balance equations. Due to the convergence problems, the multi grid method was used to enhance numerical stability. The momentum and turbulence equations were solved with a coupled tri-diagonal matrix solver (TDMA). All fluid properties were treated as being constant.

3. RESULTS AND DISCUSSION

At first, a model for the salt-water solution density current was examined. Figure 3 shows the height of the steady density current in comparison with the experimental data of Akiyama (1994). The height of the turbidity current was defined as the interface between the particle laden water and the lighter ambient fluid. In this figure, it can be seen that the $\overline{v^2} - f$ model has a very good agreement with the experimental data. In the experimental efforts, it is common to measure the height of this current via its brightness and by optical instruments. Therefore, in this work, we assumed that the current height is the place where the concentration is equal to 1% of the inlet concentration (as in the boundary layer approach).

Figure 4 shows the comparison between the standard $k - \varepsilon$, and $\overline{v^2} - f$ model to predict the body height of the density current. It can be seen that the $k - \varepsilon$ model, has overshoot the current height. This model overestimates the eddy viscosity near the wall, so the friction coefficient increases and causes the growth of the current height to be overshooting. Moreover, the $k - \varepsilon$ model over predicts the turbulence kinetic energy in the free shear layer and this increases the entrainment as a result of which the height of the current overshoots; however, the $\overline{v^2} - f$ model has a good agreement with the experimental data (Fig. 3).

Figure 5 shows a typical plot of the velocity vectors and concentration contours of computations. Figures 6 and 7 show the computed vertical structures of the dense underflow, which develops on an inclined bed. In the figures, the flow structures are given in a dimensionless form. That is, the vertical axis is non-dimensionalized by the local current thickness while and the horizontal axis by the layer-averaged values. The layer-averaged quantities can be calculated as follows

$$U_{ave} = \frac{\int_0^h u dy}{h} \quad (16)$$

$$C_{ave} = \frac{\int_0^h C dy}{h} \quad (17)$$

Figure 6 shows the dimensionless profiles of computed fractional density. A fair collapse of the computed solution is obtained for both models. Figure 7a shows a comparison between the $k - \varepsilon$ and $\overline{v^2} - f$ models in the prediction of velocity profiles at some downstream locations (dimensional form). It can be seen from Fig.7a that the maximum velocity occurs quite close to the channel bed, which is consistent with the experimental observations of Garcia (1993). Also in Fig. 7b, the velocity profiles in non-dimensional form have been shown. It can be seen that the non-dimensional forms of velocity profiles calculated by both $\overline{v^2} - f$ and $k - \varepsilon$ models have roughly agreement with the experimental data. These types of comparisons are very common in numerical and experimental efforts, but in Fig. 4, it is seen that the $k - \varepsilon$ model has over-predicted the height of the current. Then, probably, non-dimensionalizing by dependent variables (Such as h and U_{ave}) may change the structure of the current.

Three dimensionless profiles of turbulent characteristic (at $x = 3$ m) were given in Fig. 8, respectively. The dimensionless variables in this figure are defined as

$$u^* = \frac{\sqrt{\tau_w}}{\rho}; \quad y^+ = \frac{\rho u^* y}{\mu}; \quad u^+ = \frac{u}{u^*}; \quad k^+ = \frac{k}{(u^*)^2}$$

In this figure it is seen that the maximum turbulent kinetic energy occurred at the free shear layer region; however, the $k - \varepsilon$ model has a larger estimation in the turbulent kinetic energy than the $\overline{v^2} - f$ model. Due to our mesh generation, at the first five grids near the wall, y^+ is equal to u^+ and this fact shows that this model needs the denser mesh (first mesh at $y^+ \approx 1$) near the solid wall, in comparison with the $k - \varepsilon$ model, especially at the sub-layer of the boundary layer (the $k - \varepsilon$ model requires only one mesh in this region).

3.1 Entrainment concept

Due to the shear layer at the interface of turbidity current and ambient fluid, it disturbs and entrains the surrounding

fluid. Turbulence at this boundary entrains the stationary ambient fluid immediately above it into the layer and dilutes it. The turbulent region grows with distance downstream as the non-turbulent fluid becomes entrained in it. Therefore, a small mean vertical velocity perpendicular to the mean flow is generated when the ambient fluid is initially at rest. Ellison and Turner (1959) suggested that the velocity of the inflow into the turbulent region must be proportional to the velocity scale of the layer; the constant of the proportionality is called the entrainment constant E .

If 2-D flow is considered and, therefore, if the lateral entrainment is neglected, the entrainment coefficient E is defined as

$$\frac{d(UA)}{dx} = EU_{ave}b_o \quad (18)$$

Where A =area of cross section of the dense layer; U_{ave} =mean velocity of the layer; and b_o =width of the layer.

Entrainment is governed by the bottom slope, friction, and mixing at the interface of the dense layer. This mixing mechanism is parameterized by the overall Richardson number defined as

$$Ri = \frac{g'h\cos\theta}{U_{ave}^2} \quad (19)$$

where $g' = g(\rho - \rho_w) / \rho_w$; h =height of the dense layer; and θ =angle of the bed slope.

Parker (1987) showed that this functional relationship could be represented most accurately by

$$E = \frac{0.075}{(1 + 718Ri^{2.4})^{0.5}} \quad (20)$$

In this study, the entrainment coefficient is derived by

$$E = \frac{1}{U_{ave}} \frac{d}{dx}(U_{ave}h) \quad (21)$$

where h is the local height of the current.

The entrainment coefficient and height of the turbidity current, calculated with the $\overline{v^2} - f$ model are shown in Fig 9. over the length of channel for $Re_{in} = 3340$. It can be seen that E is maximum at the inlet, due to the highest shear rate; then it decreases to a constant, as the flow becomes established. Figure 10 shows the computed entrainment coefficient (close diamond) as a function of bulk Richardson number. In the figure, measured values by Parker *et al.* (1987) and Ashida and Egashira (1977) are also given, and those are represented by the open squares, respectively. The curve in the figure comes from Eq. (18), which is the best fit of the experimental results by Parker *et al.* (1987). Moreover in the figure, computed values by Choi and Garcia (2002) are also given, and those are represented by the fill circles, respectively. It is seen that the computed entrainment coefficient falls well within the range of the measured values (the experimental data has a very wide range).

3.2 Deposition rate

The deposition rate w is the rate of the particles deposition and is calculated using the following concept. The mass flow rate of particles in each cross section, is

$$w(x) = \int_0^h u(\rho - \rho_w)dy \quad (22)$$

where h is the height of turbidity current. This integration can be altered to

$$w(x) = \int_0^h u(C(\rho_s - \rho_w))dy \quad (23)$$

Due to the concentration boundary condition, at the bed $\partial C / \partial y = 0$, it is assumed that the particles deposit and are removed from the computational area. Then, the former integration can be related to the deposition rate in each cross-section of the channel. Thus, the mass flow rate of the removed particles (deposited) can be determined as:

$$deposition\ rate = -\frac{dw}{dx} \left(\frac{kg}{m.sec} \right) \quad (24)$$

With this concept, the deposition rate in some different particles' settling velocities is illustrated in Fig. 11. In this figure, it is seen that the bigger particles which provide the greater source term in the concentration equation increase the deposition rate. It can be seen that the deposition rate is maximum near the inlet, and then, it decreases to a constant as flow becomes established. Similar results were examined experimentally, by Garcia (1993) and Yu *et al.* (2000).

4. CONCLUSIONS

The $\overline{v^2} - f$ model has been applied to simulate the structure of turbidity current. Momentums, continuity, mass balance of particles and turbulence equations are solved simultaneously, by the SIMPLC method without any limited or simplified assumptions. The computed water entrainment coefficients, height of the dense fluid, velocity and concentration profiles correspond well with the different experimental data sets. It was, also, shown that the settling velocity of particles has an important influence on the vertical profile of concentration and deposition rate components. Moreover, results have been compared with the standard $k - \varepsilon$ turbulence model. It has been shown that the $k - \varepsilon$ model has a poor result in simulating this current especially in calculating anisotropic effects in the near bed region and free shear layer (entrainment) characteristics.

REFERENCES

- Akiyama, J., Stefan, H.G., (1984), "Turbidity current with erosion and deposition", *J. Hydraulic Eng, ASCE*, 111(12), 1473-1496.
- Akiyama, J., Ura, M., Wang, W. (1994), "Physical-Based Numerical Model of inclined Starting Plumes", *J. Hydraulic Eng., ASCE*, 120(10), 1139-1157.
- Alavian, V. (1986), "Behavior of density currents on an incline", *J. Hydraulic Eng., ASCE*, 112(1), 27-42.
- Altinakar, M.S., Graft, W.H., and Hopfinger, E.J. (1996), "Flow structure in turbidity Current.", *J. Hydraulic Res.*, 34(5), 713-718.

- Ashida, K. and Egashira, S. (1977), "Hydraulic characteristics of thermo cline in reservoirs." *Proc., int. 17th Congress. On Hydraulic Research*, Baden-Baden, Germany, V. 2.
- Behnia, M, Parneix, S., Y. Shabany, P.A. Durbin, (1999) "Numerical study of turbulent heat transfer in confined and unconfined impinging jets", *International Journal of Heat and Fluid Flow* 20, 1-9.
- Brrs, B., and Eidsvik, K. J. (1992), "Dynamic Reynolds stress modeling of turbidity currents." *J. Geophysics Res.*, 97(c6), 9645-9652.
- Choi, S.C., Garcia, M. (2002), " $k - \varepsilon$ Turbulence Modeling of Density Currents Developing Two Dimensionally on a Slope", *J. Hydraulic Eng., ASCE*, 128(1), 55-63
- Cokljat, D., Kim, S., Iaccarino, G., Durbin, P., (2003), "A comparative assessment of the $\overline{v^2} - f$ model for recirculating flows", *AIAA*, 0765.
- Durbin, P.A., Pettersson B.A., (2001). "Statistical Theory And Modeling For Turbulent Flow", John Willey & Sons LTD, Chapter II p.109-131.
- Durbin, P., (1996), "On the $k - \varepsilon$ stagnation point anomaly". *Int. J. Heat and Fluid Flow*, 17, 89-90.
- Durbin, P. A (1995), "separated flow computations with $k - \varepsilon - \overline{v^2}$ model", *AIAA J.*, 33, 659-664.
- Durbin, P., (1991), "Near-wall turbulence closure without damping functions", *Theoretical and Computational Fluid Dynamics*, 3, 1-13.
- Durbin, P., (1993), "A Reynolds-stress model for near-wall turbulence", *J. Fluid Mech.*, 249, 465-498.
- Eidsvik, K. J., and Brrs, B. (1989), "Self-accelerated turbidity current prediction based upon ($k - \varepsilon$) turbulence", *Cont. Shelf Res.*, 9(7), 617-627.
- Ellison, T. H., and Turner, J.S., (1959), "Turbulent entrainments in stratified flows", *J. Fluid Mech.*, 6, 423-448.
- Fan, J.; Morris, G. (1992). "Reservoir Sedimentation .II: Reservoir Desiltation and Long Term Storage Capacity", *J. of Hydraulic Eng.*, 118(3), 370-384.
- Firoozabadi, B., Farhanieh, B., Rad, M., (2001), "The propagation of turbulent density currents on sloping bed", *J. of Scientia of Iranica*, 8(2), 223-235.
- Firoozabadi, B., Farhanieh, B., Rad, M (2003). "Hydrodynamics of 2-D Laminar Turbidity Current", *Journal of Hydraulic Research*, 41(6), 623-630.
- Garcia, M. (1993), "Hydraulic jumps in sediment-driven bottom current", *J. Hydraulic Eng., ASCE*, 119(10), 1094-1117.
- Hermanson, K., Kern, S., Pareneix, S. (2003), "Prediction of external heat transfer for turbine vanes and blades with secondary flow fields", *J. of Turbomachinery*, 125, 107-113.
- Iaccarino, G., (2001), "Predictions of a turbulent separated flow using commercial CFD codes", *J. of Fluids Engineering, ASME*, 123, 819-828.
- Lakehal, D., Krebs, P., Krijgsman, J., and Rodi, W. (1999), "Computing shear flow and sludge blanket in secondary clarifiers.", *J. Hydraulic Eng., ASCE*, 125(3), 253-262.
- Launder, B., Sharma, B., (1974). "Application of the energy-dissipation model of turbulence to the calculation of flow near a spinning disc". *Letters in Heat Mass Transfer* 1, 131-138.
- Lee, H.Y., and Yu, W.S. (1997), "Experimental study of reservoir turbidity current." *J. Hydraulic Eng., ASCE*, 123(6), 520-528.
- Lien F., Kalitzin, G., (2001), "Computations of transonic flow with the $\overline{v^2} - f$ turbulence model", *International Journal of Heat and Fluid Flow*, 22, 53-61.
- Lyn, D. A., Stamou, A. I., and Rodi, W. (1992), "Density currents and shear-induced flocculation in sedimentation tanks", *J. Hydraulic Eng., ASCE*, 118(6), 849-867.
- Manceau, R., Wang, M., Laurence, D., (2001), "Inhomogeneity and isotropy effects on the redistribution term in Reynolds-Averaged Navier-Stokes modeling", *J. of Fluid Mechanics*, 438, 307-338.
- Parker, G., Fukushima, Y., and Pantin, H. M., (1986), "Self accelerating turbidity currents." *J. Fluid Mech.*, 171, 145-181.
- Parker, G., Garcia, M., Fukushima, Y., and Yu, W., (1987), "Experiments on turbidity currents over an erodible bed", *J. Hydraulic Res.*, 25, 123-147.
- Parneix, S. Durbin, P., Behnia, M., (1998), "Computation of 3-D turbulent boundary layer using the $\overline{v^2} - f$ model Flow", *Turbulence and Combustion*, 60, 19-46.
- Rad, M., (1976), "The deposition of silt in reservoirs by density current", *Ph. D. Thesis*, Imperial Coll. London University, U.K.
- Rhie C.M and Chow, W.L., (1983) "Numerical study of the turbulent flow past on airfoil with trailing edge separation" *J. AIAA*, 2, 1527-1532.
- Salaheldin, T. M., Imran, J., Chaudhry, M.H., Reed, C., (2000) "Role of fine grained sediment in turbidity current flow dynamics and resulting deposits", *Marine Geology*, 171, 21-38.
- Stacey, M. W., and Bowen, A. J., (1988a), "The vertical structure density and turbidity currents: theory and observations", *J. Geophys. Res.*, 93(C3), 3528-3542.
- Stacey, M. W., and Bowen, A. J. (1988b), "The vertical structure of turbidity currents and a necessary condition for self-maintenance", *J. Geophys. Res.*, 93(C3), 3543-3553.
- Sveningsson, A, (2003), "Analysis of the performance of different $\overline{v^2} - f$ turbulent model in a stator vane passage flow", *Licentiae thesis, Department of Thermo and Fluid Dynamics, Chalmers University of Technology*, Gothenburge, Sweden.
- Sveningsson, A., Davidson. L., (2004), "Assessment of realizability constraints in $\overline{v^2} - f$ turbulence models", *J. Heat and Fluid Flow*, 25, 785-794.
- Yu, S.W., Lee, H.Y., Hsu, S.M., (2000), "Experiments on deposition behavior of fine sediment in a reservoir", *J. Hydraulic Eng., ASCE*, 126(12), 912-920.

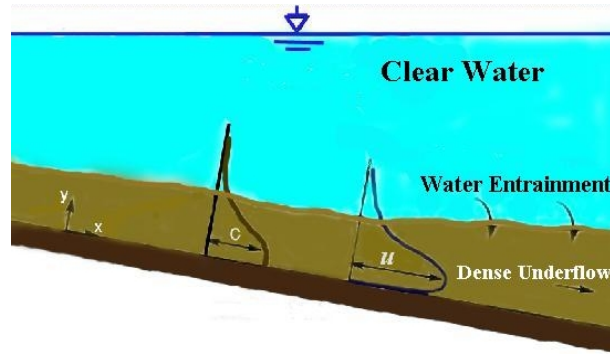


Fig. 1. The schematic sketch of the turbidity current

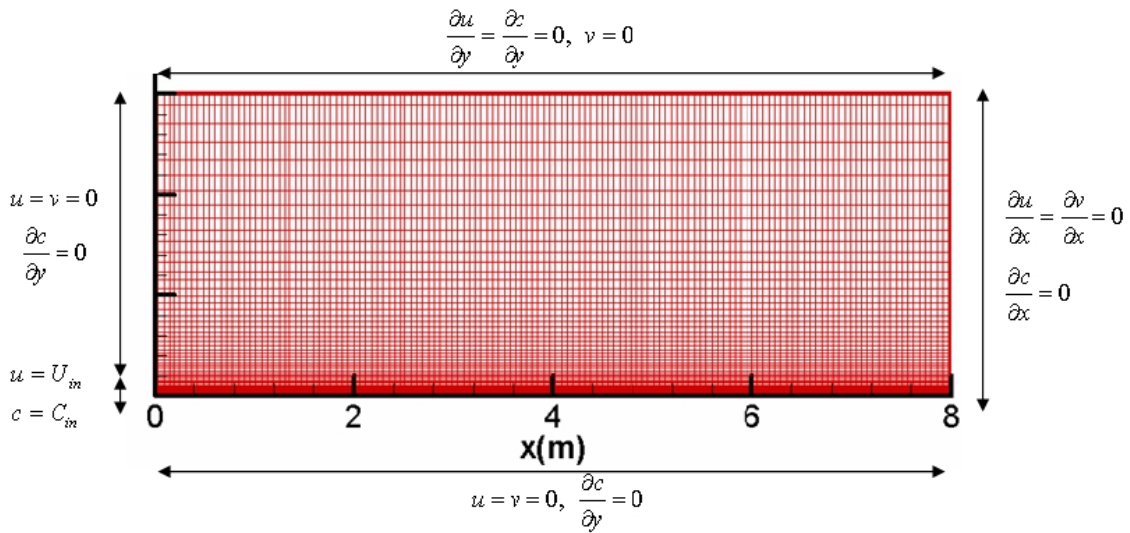


Fig. 2. The schematic sketch of grids and boundary conditions

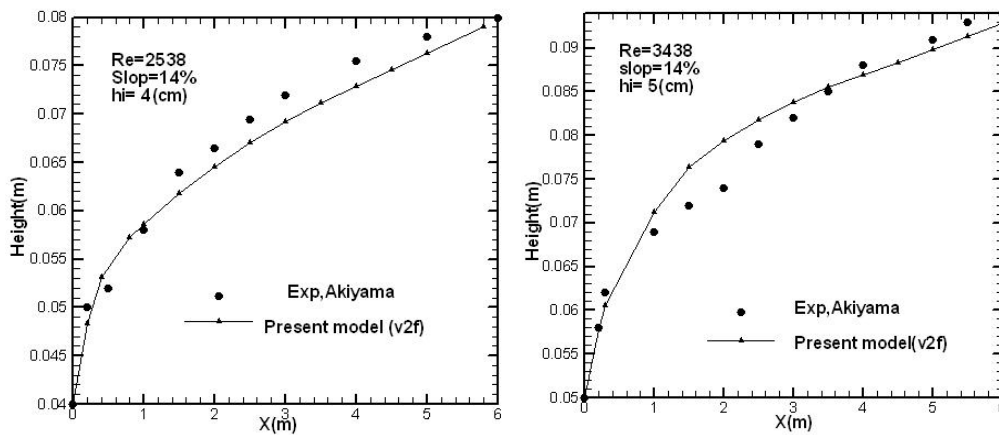


Fig. 3. The steady density current height calculated by the $\sqrt{v^2 - f}$ model, in comparison with the experimental data.

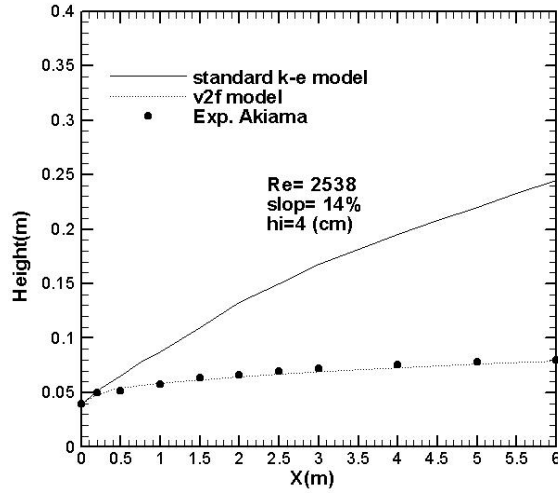


Fig. 4. The height of density current computed by the present model and standard $k - \varepsilon$

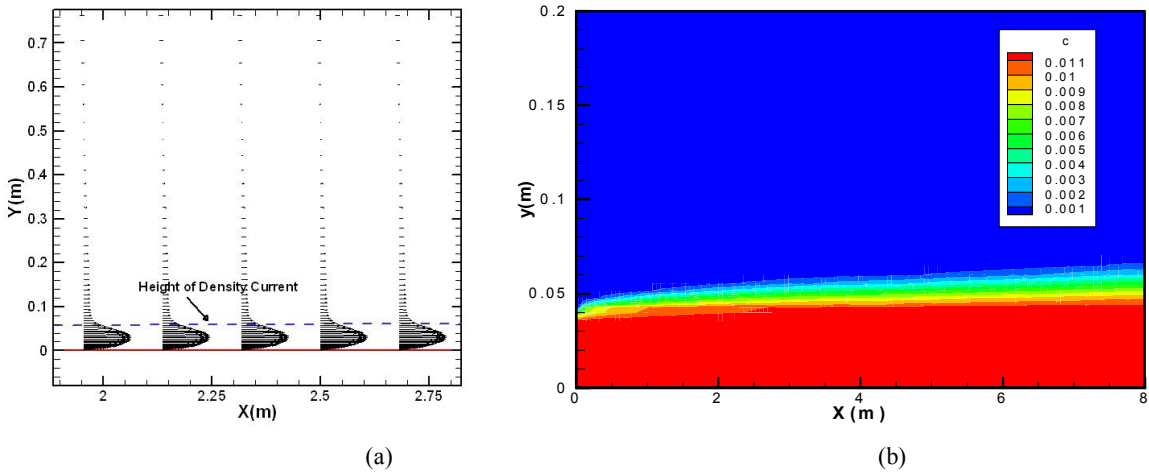


Fig. 5. The velocity vectors (a) and contour lines of concentration (b) of the turbidity current.

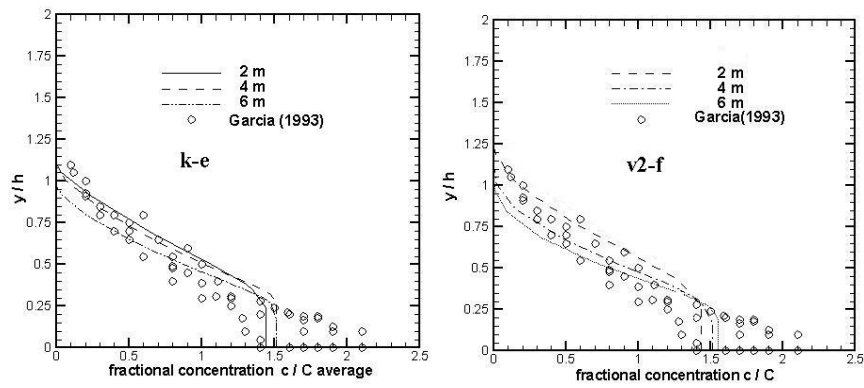


Fig. 6. Similarity collapse of vertical concentration structure of dense underflow using the $k - \varepsilon$ and $\overline{v^2} - f$ models;

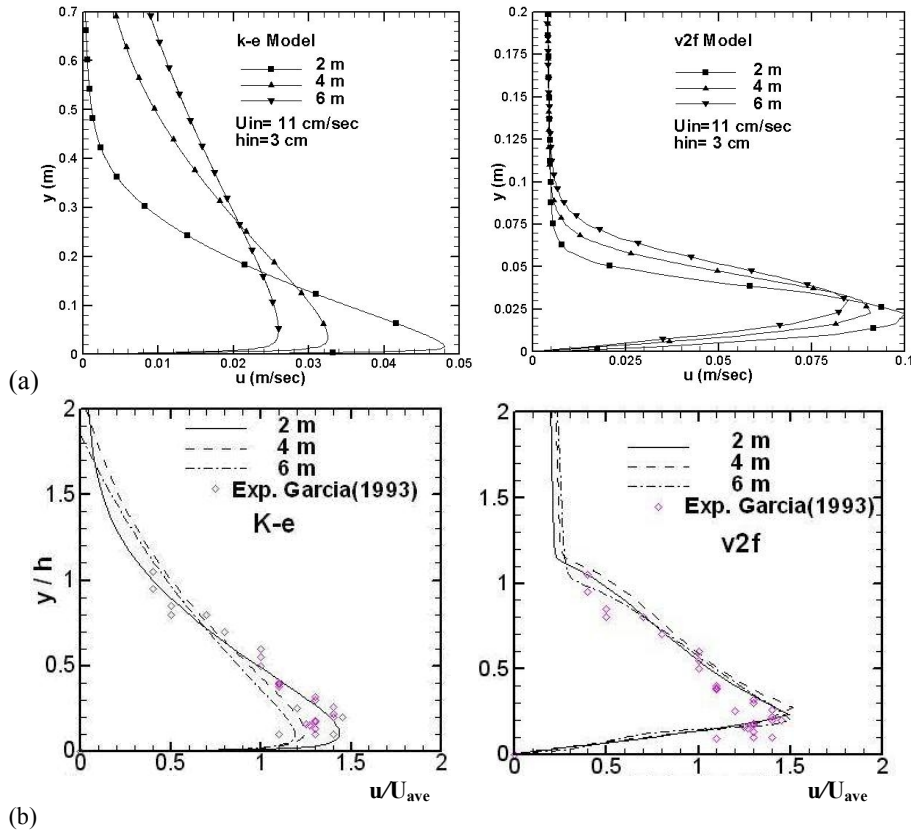


Fig. 7. Similarity collapse of vertical velocity structure using $k-\epsilon$ and v^2-f models;
a: The velocity profiles (dimensional-form) b: Non-dimensional velocity profiles

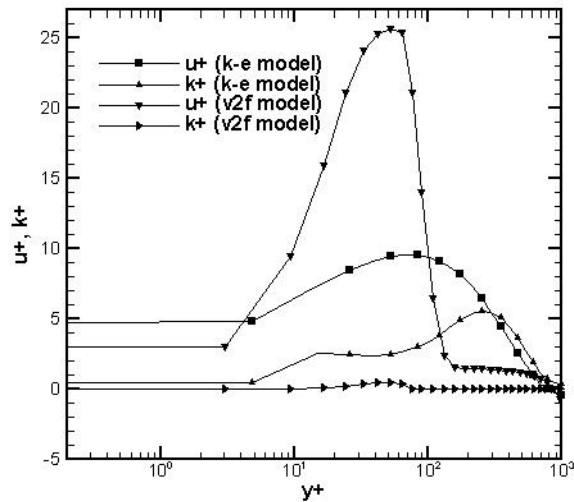


Fig. 8. Dimensionless profile of turbulent characteristic at $x=3$ (m) from the inlet

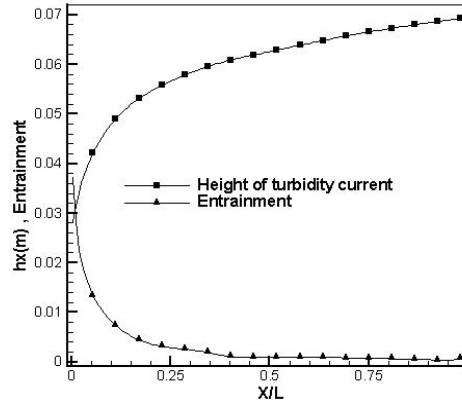


Fig. 9. The height and entrainment coefficient

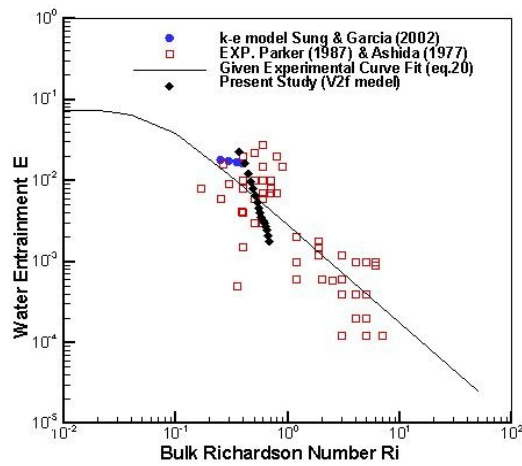


Fig. 10. Comparison of the entrainment coefficient calculated by the present model with the experimental data, and $k - \varepsilon$ model.

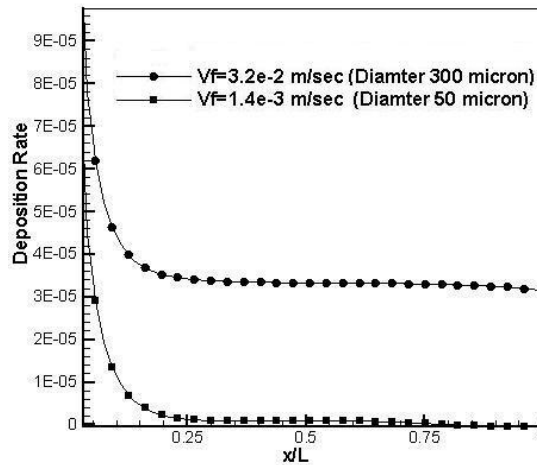


Fig. 11. Comparison of the deposition rate for two sizes of particle fall velocities